VTT Technical Research Centre of Finland

On the optimum performance of oscillating foil propulsors

Sánchez-Caja, Antonio; Martio, Jussi

Published in:
Journal of Marine Science and Technology

DOI:
10.1007/s00773-016-0397-7

Published: 01/03/2017

Document Version
Peer reviewed version

On the Optimum Performance of Oscillating Foil Propulsors

A. Sánchez-Caja[1], J. Martio[1]

[1]*VTT Technical Research Center of Finland*

Corresponding author: Antonio Sánchez-Caja, VTT Technical Research Centre of Finland, Tietotie 1A, Espoo, FI-02044 VTT, Finland. Phone: +358 50 352 4743

antonio.sanchez@vtt.fi

ABSTRACT

The design of oscillating foil propulsors is considerably more complex than that of conventional propellers due to the large amount of geometric and kinematic parameters involved in the problem. No general use of such promising propulsion concept is made routinely yet since many open questions remain to be solved. One of such questions is the sensitivity of the propulsor efficiency to foil chord length that is much larger than for conventional propellers. Our focus is on this particular problem. A potential flow theory that estimates the main force components affecting the global performance of such devices is presented. The theory is applied to oscillating foils with heaving and pitching motions and to wheel propellers with foils describing trochoidal paths. Added mass terms that usually are neglected in efficiency analyses and that play an important role in determining the global performance are included. A parameter optimization procedure is introduced in this context. Comparison to experimental data and RANS computations is made.

Key words: oscillating foil, flapping foil, foil wheel, added mass, optimization, cycloidal propellers

1. INTRODUCTION

During the last two decades much attention has been paid to the performance of oscillating foils as a propulsion concept alternative to the traditional marine propeller. High hydrodynamic efficiency was the main reason for such interest. Foil trajectories have been studied resulting from a combination of a steady

forward motion with either transverse heave motion (sinusoidal-like trajectories) or circular motion (prolate cycloidal and trochoidal trajectories). A periodic variation of pitch angle around a pivoting point is superposed on the trajectories for controlling the angle of attack of the inflow to the foil. The former trajectories are related to high thrust devices (Voit-Schneider propulsors) whereas the latter ones are related to high efficiency. Trochoidal trajectories were paid attention in the literature during the nineties but not much in recent times (Van Manen et al. [1], see literature review in Bose [2]).

Concerning foils oscillating in heave motion, experimental work was reported in Anderson et al. [3] on the NACA 0012 foil at a Reynolds number around 1100-40000. They found optimum foil performance in the range of Strouhal numbers of 0.2-0.4 and angles of attack between 20-30 deg. Read et al. [4] recorded planform-area-based thrust coefficients of 2.4 for 35-deg maximum angle of attack and efficiencies of up to 71.5% for 15-deg maximum angle of attack. A plateau of good efficiency, in the range of 50–60% was observed. However, efficiencies were not as large as those reported in the previous paper. Hover et al. [5] found that the best efficiency was to be found with the least content of high harmonics in the angle of attack, i.e. with pure sinusoidal shape, the reason of which was attributed to the production of a “pure” reverse Karman street in the wake.

From the numerical standpoint, there is a large extent of literature devoted to the investigation of flapping foil performance. Most of the studies focused on the influence of kinematic parameters such as flapping frequency, amplitude and phase difference between pure plunge and pitch motion on the thrust generation and propulsive efficiency, for example Isogai et al. [6] and Young and Lai [7]. Other studies focus on the effect of geometric parameters in foil performance like thickness and camber Garrick [8], or Cebeci et al. [9] who found a negligible effect of increasing thickness on the propulsive efficiency of a plunging airfoil or Ashraf et al. [10] who studied numerically using RANS and panel codes the effect of thickness and camber for Reynolds number ranging 200-2.000.000. He found that thickness penalizes efficiency at low Reynolds numbers but not at large ones and that camber does not affect thrust performance. Additionally, at high

Reynolds numbers thick leading edges suppress leading edge separation and consequently result in larger suction peaks. Barannyk et al. [11] investigated the influence of foil flexibility in thrust production. Vermeiden et al. [12] noticed that at high Reynolds number foil flexibility may not have significant impact on efficiency. Other research was directed to the study of pure pitching motion like in Garrick (1936) who found that for the pure pitching motion, positive thrust force can be generated only at high pitching frequency.

Concerning cycloidal propellers the number of papers in the open literature is not as large as those related to oscillating foils. However, a significant number of references can be found. For example, Tanaguchi [18], van Manen & van Terwisga [1], van Manen and van Ossanen [19], Bartels and Jürgens [20], and Jürgens and Moltrecht [21] describe the working principles of cycloidal propellers. Experimental investigations are given in Dickerson and Dobay [22], van Manen [23], Bose and Lai [24], Veitch [25] and Li [26]. Brockett [27] and Bose [2] provide a literature review of such propellers.

Some isolated applications of flapping propulsors have been recently made for full scale small vessels [13]. The high hydrodynamic efficiency claimed for such devices is due to the use of a large propulsive area (low loading), much larger than that of conventional propellers, resulting from thrusting foils extending over the ship breadth. However, the foils require the installation of supporting struts, which increase the hull resistance, and in addition the mechanic efficiency of the device is expected to be lower than that of conventional propellers. Therefore, these drawbacks should be properly accounted for within the overall ship design so that the benefits of the improved hydrodynamic performance are not obscured in practical applications. Nowadays, no general use of such promising propulsion system is applied routinely yet since many questions still remain to be solved.

Recently, in Vermeiden et al. [12], a flapping propulsor was designed for a container ship and efficiency variations were measured at a higher Reynolds number (200.000) by varying systematically loading, pitching amplitude, chord-length, chordwise flexibility and fin-spacing. An optimal configuration was found

for low chord-heave ratios operating at high transverse acceleration for maximum angles of attack of 10-11 deg. An unexpected result of the tests was the strong decrease of efficiency with growing chord-heave ratios, which cannot be explained by considerations on aspect ratio, reduced frequency or viscous losses. The chord-heave ratios were increased in an attempt to reduce accelerations. A lack of attention in the technical literature to this important phenomenon was noticed by the authors (see written discussion of the paper), in terms of either magnitude of impact or tested parametric range.

We intend to gain an insight into this problem in particular, and into foil motion optimization in general by focusing on information provided by potential flow theory with viscous corrections. Potential flow theory is known to work in global sense for the simulation of propeller flows and is used here to provide an insight in the particular problem of chord length impact on efficiency. The advantage of potential flow theory is that the effect of different components contributing to the generation of forces (camber, angle of attack, added mass) can be added linearly, which allows us to discern the causes of particular hydrodynamic phenomena.

The numerical approach is explained in section 2. This section includes also a subsection named “parameter optimization”, which is intended to facilitate the comparison of the hydrodynamic efficiency at a given thrust when the foil chord length is doubled in the propulsion unit. One parameter (for example, the foil maximum angle) is changed until the thrust of the device with a modified chord length is equal to the thrust of the original device. For the sake of completeness the optimization procedure is extended to the case were a two or three parameter optimization is desired, even though multi-parameter optimization is not needed for the present purpose of the paper. In section 3, the results of the theory are confronted with experiments for a flapping foil configuration and with URANS computations for a foil wheel device since for this latter case there are no experiments available in the open literature.

2. NUMERICAL APPROACH

2.1 POTENTIAL FLOW MODEL

Potential flow theory is used in a simplified way for optimization purposes and is intended mainly for full scale analysis where viscous effects are less critical. The foil is approximated as a wing with flat plate sections. Two-dimensional thin profile theory is coupled to lifting line theory to model the three-dimensional flow. Unsteady effects are accounted for by using Theodorsen's function which results in a lift deficiency factor and a phase lag in forces/moments. Added mass (non-circulatory) effects are modeled assuming that the foil is a flat plate heaving and pitching. Three-dimensional effects on lift and drag coefficients are modeled according to lifting line wing theory at near optimum conditions of induced drag with corrections based on tests with rudders. Drag and lift breakdown are simulated assuming a standard behavior for angles larger than the stall angle. The stall angle can be estimated by an empirical equation based on thickness chord ratio or given as an input.

Oscillating Foil

Figure 1 shows the nomenclature used in this section. A foil is moving with a vertical heave h translation and pitch rotation θ about a pivot point in the presence of a horizontal inflow V_A. The pivot point is located at a distance a from the leading edge along the chord line. The foil has a chord c and a span s. Due to the foil motions, the instantaneous angle of attack α of the relative inflow V_E to the foil is a function of flow angle β which in turn consists of two components, one due to the heave motion (β_h) and the other due to the pitch rotation (β_p). The frequencies of heave and pitch $n=\omega/2\pi$ are the same but a phase difference of the pitch over the heave motion ψ may exist. A circulatory lift L perpendicular to the relative inflow and a viscous drag D in the direction of the relative inflow are generated. The projection of these forces on the direction of motion contribute to the production of thrust for $\beta>\theta$ (or $\alpha<0$), and their projection on the vertical direction, to a vertical force F_Z responsible for power consumption. Note that Fig. 1 is made as such only for illustration purposes on the nomenclature, but in a real

application the angle β should be larger than θ in order to have a positive thrust. The effective inflow is

$$V_E = \sqrt{\begin{matrix}\left(V_A + \dot{\theta}(\tfrac{3}{4}c - a)\sin\theta\right)^2 \\ + \left(-V_Z + \dot{h} - \dot{\theta}(\tfrac{3}{4}c - a)\cos\theta\right)^2\end{matrix}} \tag{1}$$

$$\beta = \arctan\left[\frac{-V_Z + \dot{h} - \dot{\theta}(\tfrac{3}{4}c - a)\cos\theta}{V_A + \dot{\theta}(\tfrac{3}{4}c - a)\sin\theta}\right] \tag{2}$$

An additional lift L_{AM} due to added mass will be present acting on the vertical direction (Katz and Plotkin, [14]). The circulatory 2D lift L and added mass lift can be expressed from thin profile theory as

$$L = F\pi\rho V_E^2 cC(k)\left[\theta - \beta\right] \tag{3}$$

$$L_{AM} = \tfrac{1}{4}\pi\rho c^2(V_A\dot{\theta} - \ddot{h} + (\tfrac{c}{2} - a)\ddot{\theta}) \tag{4}$$

Similarly a circulatory moment Q and an added mass moment Q_{AM} are expressed as

$$Q = F\,\tfrac{\pi}{4}\rho c^2(\tfrac{4a}{c} - 1)V_E^2 C(k)\left[\theta - \beta\right] = Lc(\tfrac{a}{c} - \tfrac{1}{4}) \tag{5}$$

$$Q_{AM} = -\frac{\pi\rho\, c^2}{4}\left[\begin{matrix}(a - \tfrac{c}{2})\ddot{h} + (\tfrac{3}{4}c - a)V_A\dot{\theta} \\ + \tfrac{c^2}{4}(\tfrac{9}{8} + \tfrac{4a^2}{c^2} - \tfrac{4a}{c})\ddot{\theta}\end{matrix}\right] \tag{6}$$

where V_Z is a possible vertical inflow which will be assumed zero, ρ is the fluid density and $C(k)$ is Theodorsen's complex function accounting for the unsteady wake effect in the form of a lift deficiency factor and phase lag. Equations (3) and (5) are based on the theoretical slope of two-dimensional lift coefficient versus angle of attack, 2π. The slope is corrected by a factor F for 3D effects using

results of lifting line theory, as indicated later. For vortices shed in the wake departing noticeably from the OX axis, the distance between vortices and control points will be larger than for straight wakes, which will result in a lift deficit not as strong as that predicted by Theodorsen theory. Such effect could be approximated by applying a percentage of the estimated lift deficit for large Strouhal numbers (*St*), and could be a topic for further research

$$St = \frac{\omega h_0}{\pi V_A} \tag{7}$$

The harmonic heave and pitch oscillations can be expressed in complex form

$$h = \mathrm{Re}\left\{h_0 e^{i(\omega t - \pi/2)}\right\} \qquad \theta = \mathrm{Re}\left\{\theta_0 e^{i(\omega t + \psi - \pi/2)}\right\} \tag{8}$$

and then introduced into equations (5) and (6) to yield the phase shift and reduction of circulatory lift and moment after multiplication by *C(k)*. The reduced frequency *k* is given by

$$k = \frac{\omega c}{2V_A} \tag{9}$$

The 3D thrust *T*, vertical force F_Z and moment about the pivot point Q_{OY} are evaluated as follows,

$$F_Z = \overline{L}\cos(\beta) - \overline{D}\sin(\beta) + L_{AM}\, s \tag{10}$$

$$-T = F_X = \overline{L}\sin(\beta) + \overline{D}\cos(\beta) \tag{11}$$

$$Q_{OY} = \overline{Q} + Q_{AM}\, s \tag{12}$$

Here $\overline{L}, \overline{D}, \overline{Q}$ means 3D overall circulatory lift, drag and torque. In order to account for 3D effects, following lifting line theory, the circulatory terms in (3) can be expressed as

$$\overline{C}_L \approx \frac{2\pi(\theta - \beta)A}{(A+2)} \qquad \overline{C}_L \approx \frac{1.95\pi(\theta - \beta)}{(1+3/A)} \tag{13}$$

The equation on the left is the theoretical lift for an optimum wing of aspect ratio A in uniform flow at an angle of attack $\theta-\beta$. The equation on the right is an alternative formulation suggested by Molland and Turnock [25] which represents a satisfactory mean line through available rudder data. The latter is used in this work. The factor F in (3) and (5) can be expressed as the ratio of the 3D lift coefficient in equation (13) and the theoretical 2D lift coefficient.

An additional correction to the inflow has been implemented in the calculation inspired in propeller lifting line theory. The thrust and lateral forces induce axial (U_A) velocities that should be added to the inflow for the estimation of effective angles of attack. The axial induced velocity has been estimated by propeller momentum theory [15],

$$U_A = \frac{V_A}{2}\left(-1+\sqrt{1+C_T}\right) \tag{14}$$

where C_T is the thrust load coefficient based on the area swept by the foil, i.e. length of heave stroke ($2h$) multiplied by foil span (s).

Analogously, the overall drag coefficient can be calculated as follows,

$$\overline{C}_D = \frac{\overline{C}_L^2}{\pi e A} + \overline{C}_{D0} \tag{15}$$

The first term is the induced drag, which results from lifting line analysis of optimum wings with aspect ratio A, and the second one is a viscous drag depending on Reynolds number. The efficiency factor e is introduced into the induced drag term to bring predictions using the drag equation into line with the experimental data (Molland and Turnock, [16]).

The effective (PE) and delivered (PD) power are calculated as follows,

$$PE = TV_A \qquad PD = -F_Z\dot{h} - Q_{OY}\dot{\theta} \tag{16}$$

Even though performance after stall is not relevant for the chord-modification cases subject to analysis since the instantaneous angles of attack are small (around 10-12 deg), a simple model for lift and drag breakdown is included to approximate extreme cases. Curves of the lift and drag non-dimensional coefficients as a function of the angle of attack have been used for zones around and larger than the stall angle (α_{stall}). The lift curve is assumed to be parabolic from 0.8 α_{stall} to 1.2 α_{stall}, decreasing linearly to zero from 1.2 α_{stall} to 90 deg (see example in Fig. 2 for an aspect ratio A=3). For angles larger than stall, the drag curve is modified according to the equations developed by Spera [17]. The angle of thrust breakdown will decrease with the aspect ratio and can be estimated with experimental data provided in Molland and Turnock [16].

The variation of pitch angle for the single-shaft flapping mechanism in Vermeiden et al [12] is not exactly sinusoidal (the tangent of the pitch angle is sinusoidal), and consequently, a standard Fourier analysis should be made and introduced into equation (8).

Trochoidal Propeller

Figure 3 shows the nomenclature used in this section. A foil is rotating clockwise (negative θ) following a circular path on a system of reference which is translating in the OX direction with speed V_A. The foil has a chord c and a span s. The orientation of the foil is defined by an eccentricity point located at a distance r of the circle center, in such a way that the foil is always set perpendicular to the line d connecting the eccentricity point and the foil location on the circular path. For trochoidal propellers r should be larger than the radius of the circular path R. The position of the foil is defined by the angle θ relative to the OX axis. The foil is rotating in a direction opposite to θ with an angular velocity ω. The effective inflow V_E to the foil consists of the sum of the inflow at infinity V_A, the relative tangential velocity $R\omega$ and a velocity V_{pitch} induced by the rotation of the foil around a pivot point located on the circle. It has an incidence angle β relative to the tangent line. The angle of the foil relative to the tangent line is α. The angle of attack of the relative inflow to the foil is α-β. The angle of the foil relative to the OX is γ (positive direction shown in the figure). The pivot point describes the circular path and is usually located at a distance a about 0.25c ... 0.33c from the

foil leading edge (it is shown in the Figure at the trailing edge only for illustration purposes). Notice that the various angles in the figure are indicated with a sign in parentheses so that the positive direction of the angles can be easily identified. Notice also that perpendicular and parallel lines in the figure are shown with the same colour (blue, green or red).

For the evaluation of the added mass effects, the heave motion *h* of the foil in the OZ direction can be expressed in complex form as

$$h = R.e^{i(\omega t - \pi/2)} \tag{17}$$

being its real part the *z*-coordinate at time *t.*

The angle θ represents a generic location of the blade and covers the interval [-180,180] deg. From the figure the following geometric relations can be established:

$$r + R\sin\theta = d\cos\gamma \tag{18}$$

$$d^2 = R^2 + r^2 - 2rR\cos(\theta + \pi/2) \tag{19}$$

$$\cos\gamma = \frac{r + R\sin\theta}{\sqrt{R^2 + r^2 - 2Rr\cos(\theta + \pi/2)}} \tag{20}$$

$$\alpha + \theta + \gamma = \pi/2 \tag{21}$$

Notice that in the figure θ is a negative number that makes the sum in (21) equal to 90 deg.

The effective flow is:

$$V_E = \sqrt{\begin{pmatrix} V_A \sin\theta - V_Z \cos\theta + \omega R \\ -\dot{\gamma}(\frac{3}{4}c - a)\cos\delta \end{pmatrix}^2 + \begin{pmatrix} V_A \cos\theta + V_Z \sin\theta \\ -\dot{\gamma}(\frac{3}{4}c - a)\sin\delta \end{pmatrix}^2} \tag{22}$$

$$\delta = \alpha - \pi/2$$

A circulatory lift L perpendicular to the relative inflow and a viscous drag D in the direction of the relative inflow are generated. The angle of the pitch induced velocity with a line parallel to the tangent line is δ. The lift and drag are modelled in the same way as in the case of the oscillating foil.

The lift consists of a circulatory part L and an added mass part L_{AM}, and the added mass term is relevant only for motion in the transverse OZ direction for small γ angles,

$$\beta = \arctan\left[\frac{V_A \cos\theta + V_Z \sin\theta - \dot{\gamma}(\frac{3}{4}c - a)\sin\delta}{V_A \sin\theta - V_Z \cos\theta + \omega R - \dot{\gamma}(\frac{3}{4}c - a)\cos\delta}\right] \tag{23}$$

$$L = F\pi\rho V_E^2 c C(k)[\alpha - \beta] \tag{24}$$

$$L_{AM} = \tfrac{1}{4}\pi\rho c^2(-V_A\dot{\gamma} - \ddot{h} - (\tfrac{c}{2} - a)\ddot{\gamma}) \tag{25}$$

Similarly a circulatory moment Q_P and an added mass moment Q_{AM} around the pivot point are approximated as

$$Q_P = F\tfrac{\pi}{4}\rho c^2(\tfrac{4a}{c} - 1)V_E^2 C(k)[\alpha - \beta] = L(a - \tfrac{c}{4}) \tag{26}$$

$$Q_{AM} = -\frac{\pi\rho\, c^2}{4}\begin{bmatrix}(a - \frac{c}{2})\ddot{h} - (\frac{3}{4}c - a)V_A\dot{\gamma} \\ -\frac{c^2}{4}(\frac{9}{8} + \frac{4a^2}{c^2} - \frac{4a}{c})\ddot{\gamma}\end{bmatrix} \tag{27}$$

where V_Z is a possible vertical inflow which will be assumed zero, ρ is the fluid density and $C(k)$ is Theodorsen's complex function. In L and Q_P, the theoretical slope of the lift coefficient versus angle of attack is 2π, which can be corrected by a factor F for 3D effects as in the case of the oscillatory foil.

The added mass analysis over trochoidal paths is made for heave amplitude equal to the rotor radius and pitch amplitude of

$$\gamma_{\max} = \arcsin(R/r) \tag{28}$$

Note that the variation of pitch angle γ for the trochoidal propusor is no longer sinusoidal as was the case of the oscillating foil.

The forces are obtained from a quasi-steady analysis which results from combining the inflow velocities and the angular speed of the rotor with the geometrical setting of the blades. The unsteady interaction of the free vortex system between blades is neglected. The only interaction considered is that from the average induced velocities generated by the propulsive forces at the rotor location with the main flow in a similar way as it is done in oscillating foil case.

The projection of these forces on the direction of motion contributes to the production of thrust and the projection on the tangent line direction, to the production of torque Q responsible for power consumption.

$$T = F_X = L\cos(\theta+\beta) - D\sin(\theta+\beta) \tag{29}$$

$$F_Z = L\sin(\theta+\beta) + D\cos(\theta+\beta) + L_{AM}\,s \tag{30}$$

$$Q = M_{OY} = R(L\sin\beta + D\cos\beta) \tag{31}$$

For a pivot point at ¼ chord from the leading edge Q_P vanishes and the delivered power can be expressed as

$$PD = Q\omega + PQ_{am} + F_{Zam}V_Z \tag{32}$$

where the first term on the RHS is the circulatory power, the second one is the added mass power due to the foil motion around the pivot point and the third one is the added mass power due to the vertical motion of the foil. The circulatory and added mass terms have been calculated based on the same principles of the oscillating foil.

Parameter optimization

This section is intended to facilitate the comparison of the hydrodynamic efficiency at a given thrust when the foil chord length is doubled in the propulsion unit. One parameter (for example, the foil maximum angle) is changed until the thrust of the device with a modified chord length is equal to the thrust of the original device. For the sake of completeness the optimization procedure is extended to the case were a two or three parameter optimization is desired, even though multi-parameter optimization is not needed for the present purpose of the paper.

For a given thrust T_0 a parametric optimization was made using one, two or three parameters as described in Table I. One-parameter optimization is simply to find the magnitude of the parameter *(p)* that yields a given thrust. Following Newton-Raphson's method, the value of the parameter can be found iteratively,

$$p_{n+1} = p_n - \frac{T(p) - T_0}{T'(p)} \qquad (33)$$

Two-parameter optimization *(p,q)* requires finding the value of the parameters that minimizes power P for a given thrust T_0. We build the auxiliary function H

$$H(p,q) \equiv P + \lambda(T - T_0) \qquad (34)$$

where λ is a Lagrange multiplier, and then the optimum is given by the solution of the following equations for p, q, and λ

$$\begin{aligned} P'_p + \lambda T'_p &= 0 \\ P'_q + \lambda T'_q &= 0 \\ T - T_0 &= 0 \equiv F \end{aligned} \qquad (35)$$

The two first equations can be combined as follows,

$$\frac{P'_p}{T'_p} - \lambda \frac{P'_q}{T'_q} = 0 \equiv G \qquad (36)$$

and the parameters can be found iteratively,

$$p_{n+1} = p_n - \frac{GF'_p - FG'_p}{G'_p F'_q - F'_p G'_q}$$

$$q_{n+1} = q_n - \frac{FG'_q - GF'_q}{G'_p F'_q - F'_p G'_q} \qquad (37)$$

Alternatively, the optimum can be found by two one-dimensional optimization iteration loops within a global loop for a given thrust and given power derivative (zero),

$$p_{n+1} = p_n - \frac{T(p,q) - T_0}{T'(p,q)}$$

$$q_{n+1} = q_n - \frac{P'_q(p,q)}{P''_{qq}(p,q)} \qquad (38)$$

If the optimization of a third parameter *r* is required, the procedure can be easily extended either by adding an additional equation

$$\frac{\partial P}{\partial r} + \lambda \frac{\partial T}{\partial r} = 0 \qquad (39)$$

for the former procedure, or alternatively, an additional iteration loop

$$r_{n+1} = r_n - \frac{P'_q(p,q)}{P''_{qq}(p,q)} \qquad (40)$$

for the latter one.

The procedure can be also easily extended to the chord length optimization.

2.2 VISCOUS MODEL

In this section the URANS code used for the validation of the foil wheel case is summarized. The flow simulation is made with RANS solver FINFLO. The solution of the RANS equations is obtained by either the pseudo-compressibility method or the pressure correction method.

The spatial discretization is carried out by a finite volume method. Second- and third-order upwind-biased (MUSCL) schemes are used for the discretization of the convection terms and a second-order central-difference scheme is utilized for the diffusion. The pressure gradient is centrally differenced and a Rhie-Chow type dissipation is applied. A multigrid method is used for the acceleration of convergence. Solutions on coarse grid levels are used as starting point for the calculation in order to accelerate convergence. A detailed description of the numerical method including discretization of the governing equations, solution algorithm, boundary conditions, etc. are described by Sánchez-Caja et al. [28] and by Miettinen and Siikonen [29]. Several turbulence models are implemented in FINFLO. In these calculations Chien's low Reynolds number k- turbulence and the k-omega model turbulence model are used. Time-accurate calculations are started by using a quasi- steady solution as the initial guess. In the time-accurate calculations part of the grid is rotating at the propeller rotational speed and part of the grid is stationary. The sliding mesh technique is used to treat the interface between the rotating and the stationary part of the grid. The variables are interpolated on the sliding boundary using the solution in the neighboring blocks.

3. VALIDATION AND STUDY CASES

Oscillating Foil

Predictions of thrust versus efficiency for an oscillating foil propulsor using the proposed potential flow model with viscous corrections are presented in Fig. 4 and compared to experiments conducted in Vermeiden et al. [12]. The aspect ratio of the foil is 5.2 and the chord/heave stroke (twice heave amplitude) ratio 0.228. The phase difference between heave and pitch is 90 deg. The foil is rigid and the pivot point for the pitching motion is located at x/c=0.33 from the leading edge.

The trends of C_T-efficiency for various J_c were reasonably captured. The C_T coefficient is the thrust coefficient based on the area swept by the foil, which is related to the impulse losses in actuator disk theory. J_c is the critical advance ratio of a flapping mechanism machine, as described in the quoted reference, which is defined as follows,

$$J_c = \frac{\pi}{\tan\theta_0} \qquad (41)$$

being θ_0 the pitching amplitude.

The approach is able to disclose the reason why the fin efficiency diminishes rapidly with increasing chord length especially at low C_T. Such decrease was not possible to be attributed to the change of aspect ratio since the lift and span both do not vary, and therefore the shed vorticity remains constant at constant thrust coefficient. The decrease in efficiency could also not be explained by a total lift reduction and delay at unchanged viscous losses because the required lift is simply generated through a higher angle of attack. The explanation comes from added mass considerations. The added mass in principle is expected not to contribute to efficiency for 90 deg phase lag (see written discussion in Vermeiden et al. [12]. However, this statement is only true for foil pivoting points located at mid-chord. For pivoting points located at one-quarter chord, which is approximately optimum from the standpoint of circulatory moment minimizing, the system should expend energy to overcome the non-zero moment generated by the added mass effect by the heave motion.

Additionally, in order to correctly capture the pitching moment, the induced angle of attack due to pitch motion should be accounted for in the simulation model with sufficient accuracy. For example, the pitch-induced angle of attack is doubled for double chord length, which would alter in turn the magnitude of circulatory forces.

An illustration of the added mass effect is provided next for a foil whose chord is doubled. Let's consider the case J_c=4.76 with chord/heave stroke ratios of 0.228 and 0.456 for which experimental data are available in [12]. It corresponds to a rigid foil case at S_t=0.3. In the quoted reference, the effect of doubling the chord is

measured for several J_c values but for a foil with certain degree of chord flexibility. Figure 5 compares the efficiency obtained from the model tests for a foil with some degree of chord flexibility to that obtained from the potential flow method for a rigid foil for the reference case. In principle, according to the experiments at high Reynolds number, flexible foils yield for constant C_T an increase of efficiency compared to rigid foils which is of small magnitude compared to that of modifying the chord length by a factor of two. Consequently, the selected case can be used for the efficiency analysis. Differences in Figure 5 between experiments and calculations are considered reasonable.

The potential flow method is able to discriminate the main power components affecting efficiency and evaluate their relative magnitude. A summary of predictions of variation in power components between the chord ratios for a constant thrust coefficient of 0.1 is given in Fig. 6. The optimization procedure in section 2.2 has been followed to find the angle θ_0 which yields the same thrust as that with the original chord. Constant C_T at double chord is obtained for J_c=4.3. The power is split into circulatory (*cir*) and added mass (*am*) parts as defined in section 2, and into heave (F_zV_z) and pitching (PQ) components. The main differences are in the added mass terms.

Alternatively, the required thrust can be achieved by modifying the heave frequency and keeping the θ angle untouched. The optimization procedure can be now applied to the frequency. The power consumption for the foil with double chord length increases again due to the added mass terms but not so much as in the previous case. Figure 7 compares the power consumption.

In all the cases the maximum angles of attack are around 12 deg. If the case considered in Fig. 6 is re-calculated but for the pivot point shifted from x/c=0.33 to mid-chord, the power term $(F_zV_z)_{am}$ related to added mass will be canceled in an average sense at the cost of an increase in maximum instantaneous torque and in average added mass torque.

Trochoidal Propeller

Next, the added mass effect is illustrated when the chord length of the profiles is doubled in a four bladed foil wheel propulsor with foils describing trochoidal paths. First, predictions of thrust versus efficiency using the potential flow model are compared in Fig. 8 to URANS computations made following the approach described in Section 2. The uncertainty of the RANS computations (a couple of percents in thrust and efficiency) is much smaller than the changes in order of magnitude in efficiency derived from doubling the chord. The flow is two-dimensional and the chord/diameter ratio is 0.25. The Reynold's number is 10^7, the advance coefficient, $V/(Dn)$ is J=4.41. The foil is a rigid NACA 0015 profile. The values of C_T and efficiency are reasonably captured even though differences are somewhat larger than for the reference case in the previous oscillating foil section. The C_T coefficient is the thrust coefficient based on the area swept by the foil, i.e. diameter multiplied by span.

Let's consider now a 3D case, which will be closer to what a real application would be but keeping otherwise the main working parameters the same as in the previous 2D reference case. The foil wheel propeller will be evaluated for chord/heave stroke ratios of 0.25 and 0.50 and an aspect ratio of 10. As we are not enforcing wall boundary conditions at the tips, the achieved efficiency would be representative of the performance of a wing with aspect ratio 5 and a wall boundary condition at one tip.

A summary of predictions of variation in power components between the two chord ratios for a constant thrust coefficient of 0.33 is given in Fig. 9. The optimization procedure in section 2.2 has been applied to find the eccentricity ratio r (and the related pitch amplitude) which yields the same thrust as that with the original chord. The power is split into circulatory (*cir*) and added mass (*am*) parts as defined in section 2, and into heave (F_zV_z) and pitching (PQ) components. PD is the overall circulatory delivered power. The main differences are again in the added mass terms. Here the maximum angle of attack is around 20 deg for the reference case and around 30 deg for the double chord case.

Alternatively, the required thrust can be achieved by modifying the RPM (11 percent decrease) and keeping the eccentricity ratio (and the related pitch amplitude) untouched. The optimization procedure can now be applied to the frequency. The power consumption for the foil with double chord length increases again due to the added mass terms but not so much as in the previous case. Figure 10 compares the power consumption. Here the maximum angle of attack is around 20 deg for the double chord case.

4. CONCLUSION

Generally, potential flow theories have been applied to the prediction of oscillating foil performance using different types of simplifications. One of them is the disregard of added mass effects (or more exactly, non-circulatory effects) in efficiency analysis since in principle they do not contribute to consumption or production of energy for 90 deg phase lag between heave and pitch. Such assumption is shown to be approximately valid under optimum conditions for 90 lag between heave and pitch motion. In fact, for foils pivoting around mid-chord the time-averaged heave component of added mass is zero, but not for pivoting points located around the one-quarter chord, which is the ordinary location for minimization of torque. In other words, the optimum location of the pivoting point from the standpoint of minimizing the circulatory moment is around x/c=0.25-0.3; however, from the standpoint of cancelling heave added mass effects is x/c=0.5, and the former location is usually preferred. Moreover, added mass effects due to pitching motion are not expected to vanish with pivot points located at mid-chord.

An oscillating foil and a cycloidal propeller working at near optimal conditions for which there is available either experimental or numerical (RANS) data have been analyzed using a potential flow method. The method shows that the added mass effects are small in such situation. However, when the chord is doubled and other hydrodynamic parameters are adjusted for a constant thrust condition, added mass effects start to play an important role, which results in the deterioration of foil performance. The decrease of efficiency could be partially alleviated by shifting the pivot point to mid-chord but at the risk of increasing the maximum pitching torque around the foil pivot point.

Although the approach does not consider some especial viscous effects like leading edge vortex separation, in near optimal situations at high Reynolds numbers the effective angles of attack are small and the influence of such effects is not significant. Besides it should be noticed that high efficiencies based on interaction of vortices that can be achieved only under laboratory conditions should not be pursued in real full scale applications.

Potential flow theory with viscous corrections is found to be useful for discriminating different components of forces contributing to power consumption, and consequently, for providing initial estimations of performance for different types of oscillating foils.

ACKNOWLEDGEMENTS

The authors are grateful to the support provided for the research work by the Finnish Funding Agency for Innovation TEKES.

REFERENCES

[1] van Manen, J., van Terwisga, T. A new way of simulating whale tail propulsion. 21st Symposium on Naval Hydrodynamics 1997.

[2] Bose, N. Marine Power Prediction and Propulsors. ISBN-10:0939773651 published by SNAME, 2008.

[3] Anderson, J. M., Streitlien, K., Barrett, D. S., Triantafyllou, M. S., 1998. Oscillating foils of high propulsive efficiency. Journal of Fluid Mechanics 360, 41–72.

[4] Read, D. A., Hover, F. S., Triantafyllou, M. S., 2003. Forces on oscillating foils for propulsion and maneuvering. Journal of Fluids and Structures 17 (1), 163–183.

[5] Hover F, Haugsdal Ø, Triantafyllou M. Effect of angle of attack profiles in flapping foil propulsion. J Fluids Struct 2004; 19:37–47.

[6] Isogai, K., Shinmoto, Y., Watanabe, Y., 1999. Effects of dynamic stall on propulsive efficiency and thrust of flapping airfoil. AIAA Journal 37 (10), 1145–1151.

[7] Young, J., Lai, J. C. S., 2004. Oscillation frequency and amplitude effects on the wake of plunging airfoil. AIAA Journal 42 (10), 2042–2052

[8] Garrick, I. E., 1936. Propulsion of a flapping and oscillating airfoil. NACA Report No. 567.

[9] Cebeci, T., Platzer, M., Chen, H., Chang, K.-C. ,Shao, J. P., 2004. Analysis of Low-Speed Unsteady Airfoil Flows .Horizons Publishing Inc.

[10] Ashraf , M. A., 2010. Numerical simulation of the flow over flapping airfoils in propulsion and power extraction regimes. Canberra, The University of New South Wales at Australian Defence Force Academy. Ph. D. Thesis.

[11] Barannyk, O, Buckham, B. J., Oshkai, P. On performance of an oscillating plateu nder water propulsion system with variable chordwise flexibility at different depths of submergence. Journal of Fluids and Structures 28 (2012) 152–166.

[12] Vermeiden J. G., Kooiker, K., Lafeber, F.H. van Terwisga, T., Cerup-Simonsen B., Folsø R. A Systematic Experimental Study on Powering Performance of Flapping Foil Propulsors. 29th Symposium on Naval Hydrodynamics Gothenburg, Sweden, 26-31 August 2012.

[13] O-foil wing propulsion, the motor vessel ‘Triade’, http://www.ofoil.nl/en/news/ 2014. Also interview in the Dutch journal Schuttevaer.

[14] Katz, J. and Plotkin, A. 1991. Low speed aerodynamics: from wing theory to panel methods. McGraw-Hill series in aeronautical and aerospace engineering. ISBN 0-07-050446-6.

[15] Breslin, J.P., Andersen, P. 1994. Hydrodynamics of Ship Propellers. Cambridge university press. ISBN 0-521-41360-5.

[16] Molland, A.F., and Turnock S.R., 2007, Marine Rudders and Control Surfaces: principles, data and design, Butterworth Heineman, 414 pp.

[17] Spera, D. Models of Lift and Drag Coefficients of Stalled and Unstalled Airfoils in Wind Turbines and Wind Tunnels. NASA/CR-2008-215434

[18] Taniguchi, K., 1962. Sea analysis of vertical axis propellers. Proceedings of the 4th Symposium on Naval Hydrodynamics, Office of Naval Research, Washington, pp.429-446.

[19] van Manen, J., van Oossanen, T., 1998, Propulsion in Principles of Naval Architecture, Vol. II. SNAME, Jersey city, NY, pp.127-254.

[20] Bartels J.-E., Jürgens, D., 2000, Voith-Schneider-propeller, actual applications and new developments, in Handbuch der Werften XXVI, Schiffaluns-Verlag, Hamburg (in German).

[21] Jürgens, D., Moltrecht, T. 2002, Enhanced cycloidal propulsion. The International Workboat Show, New Orleans.

[22] Dickerson, M.C., Dobay, G.F., 1975, Experimental performance of some high pitch cycloidal propellers, Report SPD-399-01, David Taylor Naval Ship Research and Development Center, Bethesda, MD, 45 pp.

[23] van Manen, J., 1973, Non-conventional propulsion devices, International Shipbuilding Progress, Vol. 20 no.226, pp.173-193.

[24] Bose, N., Lai, P.S.K., 1989. The experimental performance of a trochoidal propeller with high aspect ratio blades. Marine Technology, Vol. 26, no.3 pp. 192-201.

[25] Veitch, B.J., 1990, Experimental results and theoretical predictions of trocoidal propeller performance. MEng thesis, Faculty of Engineering and Applied Science, Memorial University of Newfoundland, St. John's.

[26] Li, J., 1991 Theoretical and experimental study of cycloidal propellers, MEng thesis, Faculty of Engineering and Applied Science, Memorial University of Newfoundland, St. John's.

[27] Brockett, T. 1991, Hydrodynamic analysis of cycloidal propulsors in Proceedings of the Propeller Shafting '91 Symposium SNAME, Jersey city, NY, pp.127-254.

[28] Sánchez-Caja, A., Rautaheimo, P., Salminen, E., and Siikonen, T., "Computation of the Incompressible Viscous Flow around a Tractor Thruster Using a Sliding Mesh Technique," 7th International Conference in Numerical Ship Hydrodynamics, Nantes (France), 1999.

[29] Miettinen, A., and T. Siikonen. "Application of pressure-and density-based methods for different flow speeds." International Journal for Numerical Methods in Fluids (2015).

FIGURE CAPTIONS

Figure 1. Notional illustration of oscillating foil motions

Figure 2. Variation of lift and drag as function of the angle of attack for a stall angle of 20 deg.

Figure 3. Notional illustration of velocity components in a trochoidal propeller. Perpendicular lines are drawn in the same color.

Figure 4. Comparison of efficiency and thrust coefficient as predicted by potential flow theory with experiments. The uncertainty of the experiments is marked around the experimental points.

Figure 5. Comparison of calculated and measured efficiency for C_T=0.1 when the chord is doubled.

Figure 6. Change in power consumption at constant C_T when the chord is doubled. Power is split into circulatory (cir) and added mass (am) components, and into translational heave (F_zV_z) and pitching torque (PQ) components. Constant C_T is achieved by modification of pitch angle.

Figure 7. Change in power consumption at constant C_T when the chord is doubled. Power is split into circulatory (cir) and added mass (am) components, and into translational heave (F_zV_z) and pitching torque (PQ) components. Constant C_T is achieved by modification of frequency.

Figure 8. Comparison of efficiency calculated by the potential-flow based model and computed by RANS solver for the reference case.

Figure 9. Change in power consumption (W) at constant C_T when the chord is doubled. Power is split into circulatory (cir) and added mass (am) components, and into translational heave (F_zV_z) and pitching torque (PQ) components. Constant C_T is achieved by modification of pitch angle.

Figure 10. Change in power consumption (W) at constant C_T when the chord is doubled. Power is split into circulatory (cir) and added mass (am) components, and into translational heave (F_zV_z) and pitching torque (PQ) components. Constant C_T is achieved by modification of RPM.

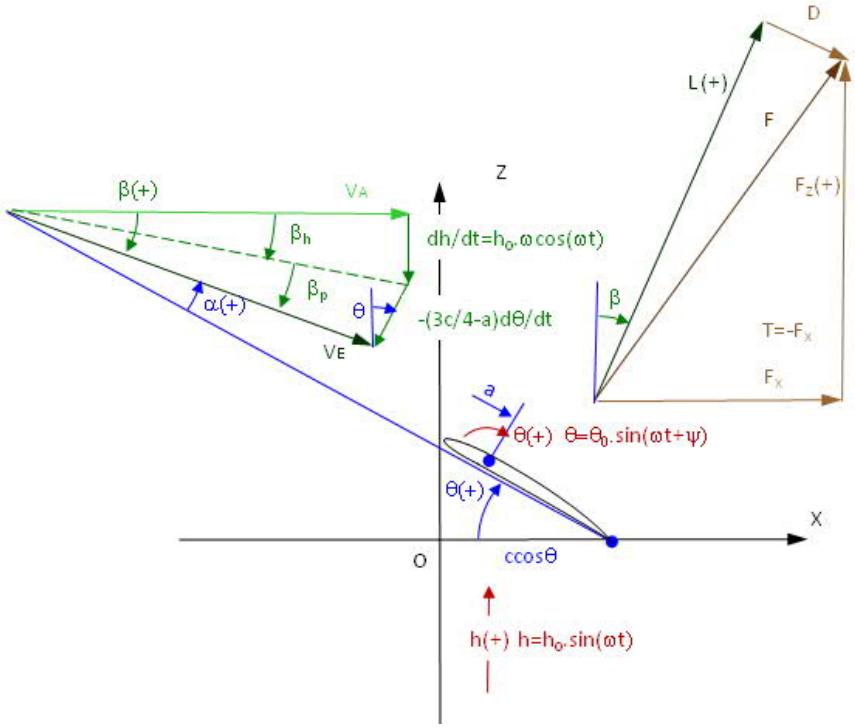

Figure 1. Notional illustration of oscillating foil motions

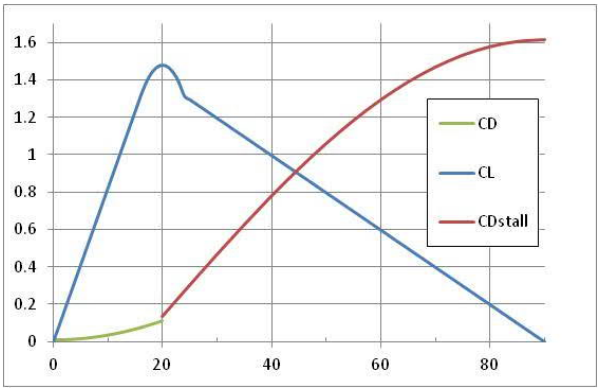

Figure 2. Variation of lift and drag as function of the angle of attack for a stall angle of 20 deg.

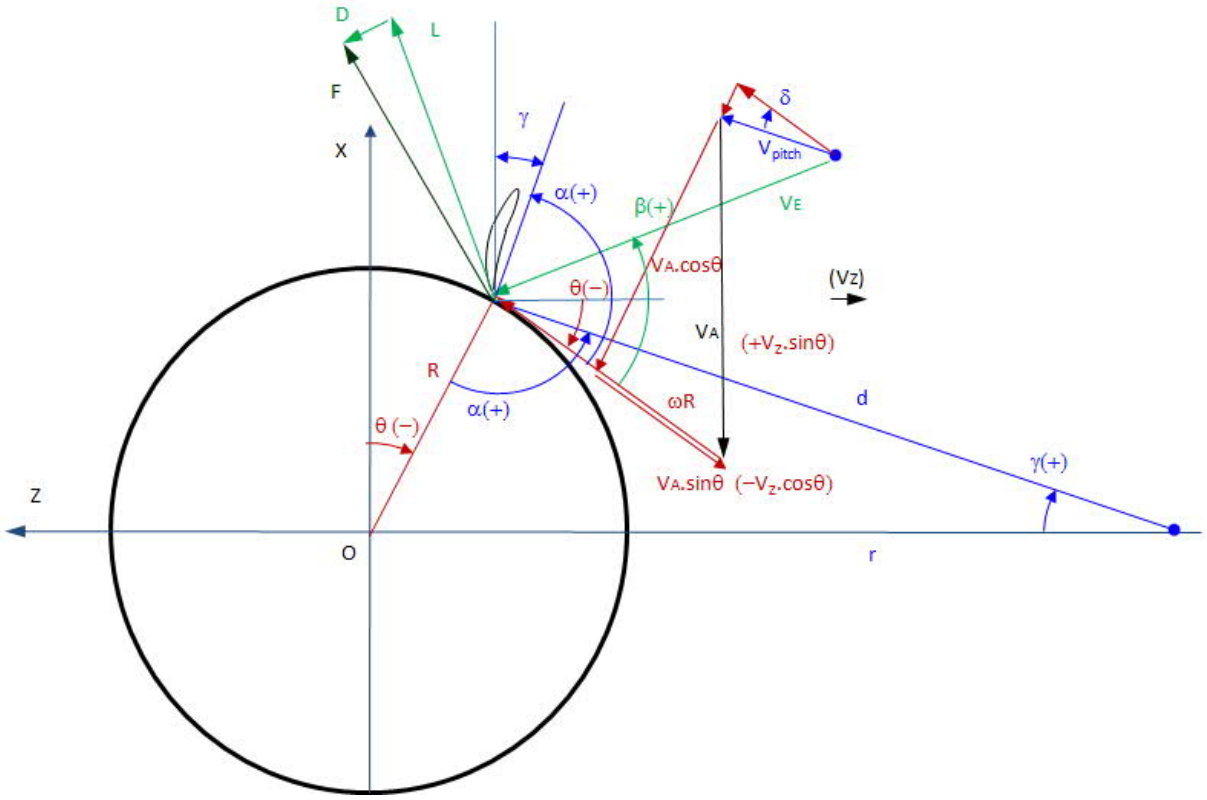

Figure 3. Notional illustration of velocity components in a trochoidal propeller. Perpendicular lines are drawn in the same color.

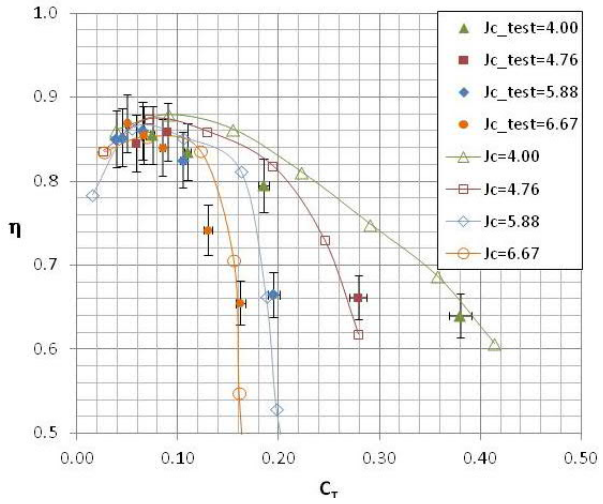

Figure 4. Comparison of efficiency and thrust coefficient as predicted by potential flow theory with experiments. The uncertainty of the experiments is marked around the experimental points.

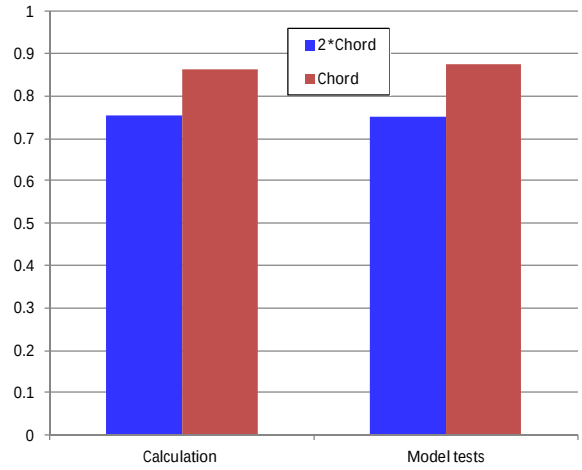

Figure 5. Comparison of calculated and measured efficiency for C_T=0.1 when the chord is doubled.

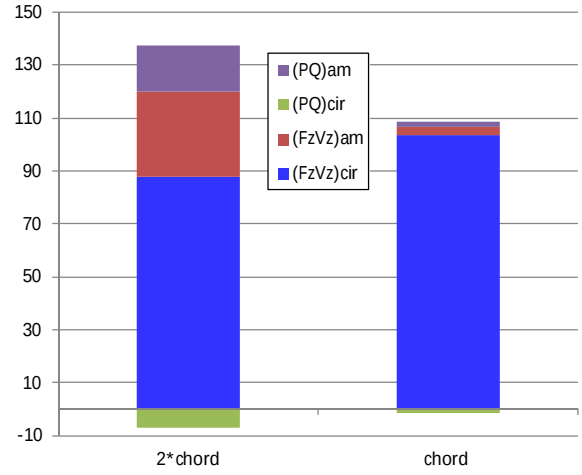

Figure 6. Change in power consumption at constant C_T when the chord is doubled. Power is split into circulatory (cir) and added mass (am) components, and into translational heave (F_zV_z) and pitching torque (PQ) components. Constant C_T=0.1 is achieved by modification of pitch angle.

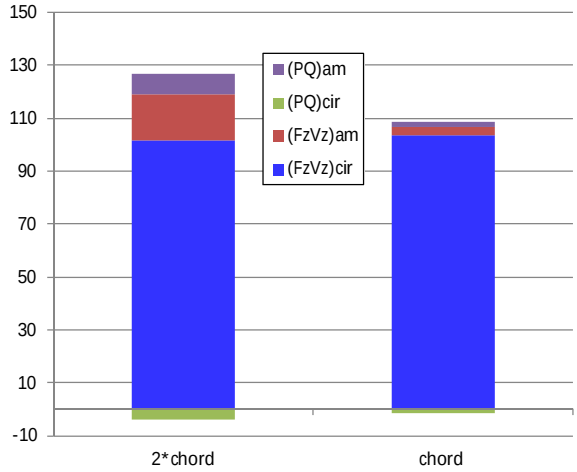

Figure 7. Change in power consumption at constant C_T when the chord is doubled. Power is split into circulatory (cir) and added mass (am) components, and into translational heave (F_zV_z) and pitching torque (PQ) components. Constant C_T=0.1 is achieved by modification of frequency.

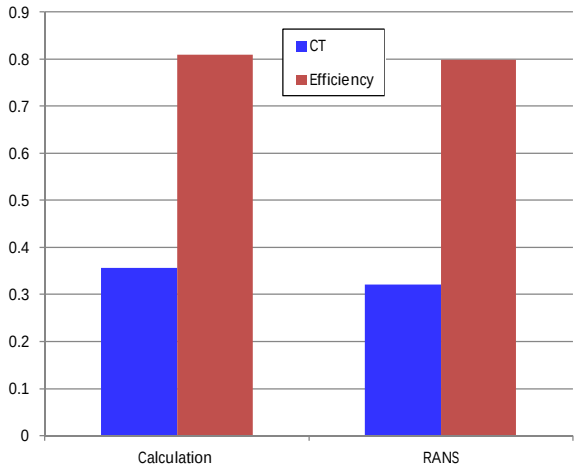

Figure 8. Comparison of efficiency calculated by the potential-flow based model and computed by RANS solver for the reference case.

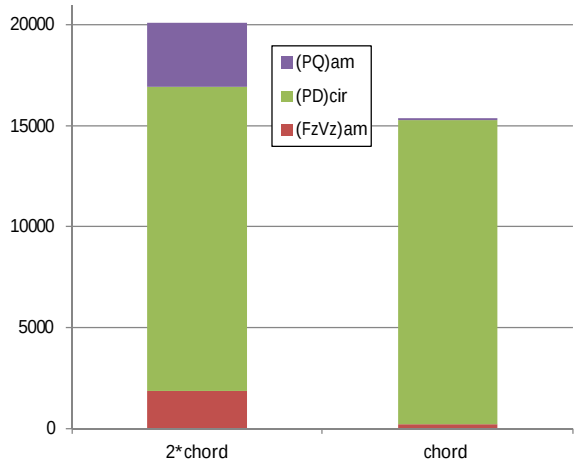

Figure 9. Change in power consumption (W) at constant C_T when the chord is doubled. Power is split into circulatory (cir) and added mass (am) components, and into translational heave (F_zV_z) and pitching torque (PQ) components. Constant C_T=0.326 is achieved by modification of pitch angle.

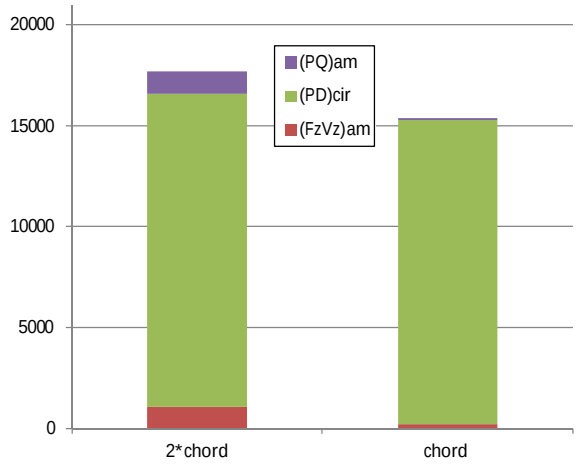

Figure 10. Change in power consumption (W) at constant C_T when the chord is doubled. Power is split into circulatory (cir) and added mass (am) components, and into translational heave (F_zV_z) and pitching torque (PQ) components. Constant C_T=0.326 is achieved by modification of RPM.

Table 1. Parameter optimization.

Oscillating foil		
1 parameter	2 parameter	3 parameter
α	α,ω	α, ω, ψ
h	h,ω	h, α, ω
ω	h,α	

Trocoidal propeller		
1 parameter	2 parameter	3 parameter
r	r,ω	r, ω, ψ
D	Diameter,ω	Diam., r, ω
ω	Diameter,r	